



Biomass-burning-derived particles from a wide variety of fuels – Part 1: Properties of primary particles^{CFI}

Crystal D. McClure¹, Christopher Y. Lim², David H. Hagan², Jesse H. Kroll², and Christopher D. Cappa^{1,3,a}

¹Department of Civil and Environmental Engineering, University of California, Davis, CA 95616, USA^{TS1}

²Department of Civil and Environmental Engineering, Massachusetts Institute of Technology, Cambridge, MA 02142, USA

³Atmospheric Sciences Graduate Group, University of California, Davis, CA 95616, USA

^anow at: Department of Chemistry, University of Toronto, Ontario, Canada

Correspondence: Crystal D. McClure (cdcappa@ucdavis.edu)

Received: 13 August 2019 – Discussion started: 15 August 2019

Revised: 9 December 2019 – Accepted: 3 January 2020 – Published:

Abstract. ^{TS2 TS3}Relationships between various optical, physical, and chemical properties of biomass-combustion-derived particles are characterized for particles produced in the laboratory from a wide range of fuels and burn conditions. The modified combustion efficiency (MCE), commonly used to parameterize biomass particle emissions and properties, is shown to generally have weak predictive capabilities, especially for more efficient combustion conditions. There is, however, a strong relationship between many intensive optical properties (e.g., single-scatter albedo, Ångström absorption exponent, mass absorption efficiency) and the organic aerosol-to-black carbon ([OA] / [BC]) mass ratio over a wider range than previously considered (0.3 to 10⁵). The properties of brown carbon (BrC, i.e., light-absorbing organic carbon) also vary with [OA] / [BC]. Coating-induced enhancements (i.e., “lensing” effects) contribute only a minor amount to BC absorption for all of the burns despite some burns producing particles having large ensemble-average coating-to-core mass ratios. The BC–OA mixing state varies strongly with [OA] / [BC]; the fraction of OA that is internally mixed with BC decreases with [OA] / [BC] while the relative amount of OA coated on BC increases. In contrast, there is little relationship between many OA bulk chemical properties and [OA] / [BC], with the O : C and H : C atomic ratios and the relative abundance of a key marker ion ($m/z = 60$, linked to levoglucosan) all showing no dependence on [OA] / [BC]. In contrast, both the organic nitrate fraction of OA and the OA volatility do depend on the [OA] / [BC]. Neither the total particle nor BC-specific size distributions exhibit any clear dependence on the burn con-

ditions or [OA] / [BC], although there is perhaps a dependence on fuel type. Overall, our results expand on existing knowledge to contribute new understanding of the properties of particles emitted from biomass combustion.

1 Introduction

While it is understood that both open and controlled biomass combustion are major sources of particles to the atmosphere (Andreae and Merlet, 2001), questions remain regarding the properties of the emitted particles, their relationship with combustion conditions and fuel type, and their atmospheric evolution. Particles emitted from biomass combustion impact the global radiation budget and contribute to poor air quality in impacted regions. The emitted primary particles are primarily composed of organic aerosol (OA) and black carbon (BC), in varying amounts, with trace inorganic species (Reid et al., 2005; McMeeking et al., 2009; Levin et al., 2010). Particle intensive properties are often compared against the modified combustion efficiency ($MCE \sim \Delta[CO_2] / (\Delta[CO] + \Delta[CO_2])$), which provides a measure of the combustion efficiency of a burn. For example, various particle properties show some relationship with MCE, but often these relationships are weak, especially for more efficient combustion (higher MCE, corresponding typically to flaming conditions) (McMeeking et al., 2009, 2014; Liu et al., 2013). Understanding the diversity in the chemical, physical, and optical properties of the emitted particles is important for establish-

ing the fire- or region-specific emissions and subsequent impacts.

The emitted OA from biomass combustion is somewhat light absorbing (Kirchstetter et al., 2004). Absorbing OA is commonly referred to as brown carbon (BrC), with properties that appear to depend on the fuel and combustion conditions (Saleh et al., 2014; Laskin et al., 2018), which affect particle organic composition (Jen et al., 2019). However, the properties of primary BrC absorption and, especially, understanding of the relationships between BrC absorption and other particle properties and burn conditions are only beginning to be unraveled. Additionally, it is established from theory and laboratory experiments that nonabsorbing coatings on black carbon and other strongly absorbing particles can enhance the absorption (commonly referred to as the “lensing” effect but more accurately termed here the coating-induced enhancement) (Fuller et al., 1999; Bond et al., 2006; Lack et al., 2009; Shiraiwa et al., 2010; Cappa et al., 2012). Yet, the extent to which coating-induced enhancements impact absorption by ambient particles or for mixed-component particles from complex sources, such as biomass burning, remains contentious (Cappa et al., 2012; Healy et al., 2015; Liu et al., 2015, 2017; Peng et al., 2016).

Here, we expand on current understanding of the relationships between various primary particle properties and burn conditions by analyzing measurements of primary biomass burning particles produced from combustion of a variety of fuel types, many of particular relevance to the western United States. We demonstrate that various optical properties exhibit a strong relationship with the [OA] / [BC] mass ratio, much stronger than their relationship with the MCE. We use the measurements to quantify the individual contributions of BC and BrC, as well as from internal mixing of BC to the observed light absorption, and we examine the variability in the properties of BrC specifically. We uniquely characterize the mixing state of BC and OA, as well as how mixing states vary between individual burns and depend on the mean properties of the emitted particles. We characterize the variability of OA-specific properties, including OA volatility, bulk chemical composition (characterized by the O : C and H : C atomic ratio, as well as the presence of key marker ions), and, uniquely, the relative abundance of organic nitrate species. We also examine the variability in the emitted particle size distribution, both for the total particles and for the BC particles specifically. Some of our analysis serves to support and extend previously determined relationships by considering a wider range of conditions, while other aspects are unique to this study. These observations provide a foundation for understanding and interpretation of experiments on the influence of photochemical aging on biomass particle properties, discussed in a related paper (Lim et al., 2019).

2 Methods

All experiments were conducted during the Fire Influence on Regional to Global Environments Experiment (FIREX) lab study, which took place at the Missoula Fire Sciences Laboratory in Missoula, MT, USA, during November, 2016. Numerous types of biomass were combusted in a large chamber (12 m × 12 m × 19 m) and the smoke was sampled to provide information on the physical, chemical, and optical properties of the resulting smoke (i.e., particulate and gas emissions). The general fuels types combusted included (exclusively or in combination) duff, dung, excelsior, straw, litter, untreated lumber, rotten debris, woody debris, shrub, herbaceous, and canopy biomass. A complete list of fuels and types is provided in Table S1 in the Supplement, with further details available on the U.S. National Oceanic and Atmospheric Administration (NOAA) data archive (<https://esrl.noaa.gov/csd/projects/firex/>). All data used in this publication are also available on the NOAA archive, with the processed data summarized in the complementary data repository (Cappa et al., 2019a).

Both “room” and “stack” burns were conducted, although here we include results only from stack burns. During stack burns, the smoke was mixed with background room air and funneled up a large cylindrical stack (2 m diameter × 15 m height) where it was sampled into a high-flow transfer line at ca. $0.27 \text{ m}^3 \text{ s}^{-1}$. This flow rate corresponded to sampling approximately 10 % of the stack flow. Smoke was transferred to an adjacent room via the high-flow transfer line (residence time ca. 2 s) where it was subsampled through a PM_{2.5} cyclone and injected into a 0.25 m³ Teflon photochemical reaction chamber (the mini chamber). Details on the construction and operation of the mini chamber can be found in Lim et al. (2019). Here, we focus exclusively on the properties of particles sampled prior to initiation of photochemical oxidation; results of the photochemical oxidation experiments are discussed in a series of papers (Coggon et al., 2019; Lim et al., 2019). In brief, prior to each burn, the chamber was flushed with clean air with a relative humidity (RH) of approximately 40 %. To fill the chamber, smoke was subsampled from the high-flow inlet and injected across the entire burn (typically lasting for 10–20 min) or until the chamber concentration reached a maximum. A suite of instruments sampled from the mini chamber at a flow rate of approximately 6 L min^{-1} . This flow rate varied from burn to burn due to the exact suite of instrument sampling. Clean makeup air was being injected simultaneously from a zero-air generator to equal the air being sampled out of the chamber. The sampled smoke was diluted by a factor of ca. 7 relative to the air in the high-flow inlet. Subsequent dilution after filling was characterized by the decay of acetonitrile (ACN). Properties of the primary particles are averaged over the 5–10 min period after filling but before the initiation of photochemistry.

Particle-phase instrumentation sampled alternately every 2 min through a thermodenuded or ambient sample line.

The thermodenuder was operated at 300 °C with a residence time of approximately 5 s and volatilized semivolatile components, including those that are internally mixed with BC. The ambient line was lined with a charcoal cloth that removed excess gases (such as VOCs, NO_x, and O₃) that could interfere with particle-phase measurements. Comparison of thermodenuded versus ambient particles allowed for the investigation of coating amount and volatility. The gas-phase composition in the mini chamber was similar to that sampled directly from the fire (Koss et al., 2018; Lim et al., 2019). Particle-phase instrumentation included a multi-wavelength cavity ring-down photoacoustic absorption spectrometer (CRD-PAS) and a photoacoustic absorption spectrometer (PASS-3) for characterization of light absorption and extinction coefficients at 405, 532, and 781 nm; a high-resolution aerosol mass spectrometer (HR-ToF-AMS) for characterization of nonrefractory submicron particulate matter (NR-PM₁) components (i.e., OA, NO₃, SO₄, NH₄, Cl, K); a soot photometer AMS (SP-AMS) in laser-only mode for characterization of refractory BC and the NR components that are internally mixed with BC; a single-particle soot photometer (SP2) for characterization of refractory BC mass concentrations and size distributions; and a scanning electrical mobility sizer (SEMS) for measurement of particle mobility size distributions. Further details regarding instrument operation and calibration are provided in the Supplement and in Lim et al. (2019).

3 Results and discussion

3.1 Bulk optical property relationships

Due to the wide variety of biomass fuels and types used during FIREX, there was a substantial diversity in the properties of primary particles produced. Previous studies have shown both the single-scatter albedo (SSA) and wavelength dependence of absorption (the absorption Ångström exponent, AAE) depend on the modified combustion efficiency (MCE) (Liu et al., 2013; McMeeking et al., 2014; Pokhrel et al., 2017). The MCE is defined here as

$$\text{MCE} = \frac{[\text{CO}_2]}{[\text{CO}_2] + [\text{CO}]}. \quad (1)$$

The SSA is defined as

$$\text{SSA} = \frac{b_{\text{ext}} - b_{\text{abs}}}{b_{\text{ext}}}, \quad (2)$$

where b_{ext} is the wavelength-specific extinction coefficient and b_{abs} is the wavelength-specific absorption coefficient. The AAE is defined as

$$\text{AAE} = -\log\left(\frac{b_{\text{abs},\lambda_1}}{b_{\text{abs},\lambda_2}}\right) / \log\left(\frac{\lambda_1}{\lambda_2}\right), \quad (3)$$

where λ_1 and λ_2 indicate two different wavelengths, here 405 and 532 nm. The MCE characterizes the overall combustion efficiency, with values closer to unity indicating more

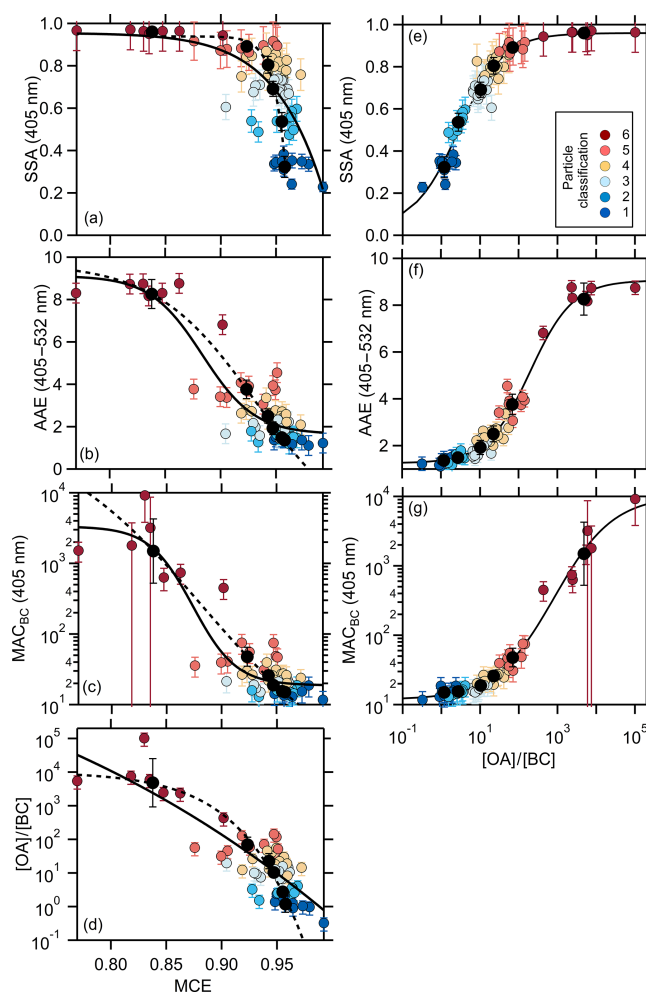


Figure 1. (a–d) Relationship between (a) the SSA_{405 nm}, (b) the AAE_{405–532}, (c) the MAC_{BC}, and (d) the [OA] / [BC] mass ratio and the modified combustion efficiency, MCE. Results for individual burns are shown as points colored by the particle class, and class average values are shown as black circles. Uncertainties on the class averages are 1σ based on measurement variability and uncertainties for the individual burns are from error propagation of measurement uncertainties. The solid black lines are fits to the individual burns (colored points) while the dashed black lines are fits to the class averages (Table S2). (e–g) Relationship between (e) the SSA_{405 nm}, (f) the AAE_{405–532}, and (g) the MAC_{BC} on the [OA] / [BC] mass ratio. The solid black lines here are sigmoidal fits to the individual burns. Fits to the class averages are similar.

complete combustion. In general, higher MCEs correspond to more flaming combustion conditions while smaller MCEs correspond to more smoldering conditions. We find a similar relationship between SSA_{405 nm}, AAE, and [OA] / [BC] with MCE to previous studies (Fig. 1) (McMeeking et al., 2009, 2014; Liu et al., 2013; Pokhrel et al., 2017). Specifically, the SSA_{405 nm} is relatively constant and near unity for MCE < ~ 0.9, but above this value it exhibits a rapid decline, albeit with a substantial amount of scatter (Fig. 1a). The AAE

is also relatively constant when $MCE < 0.9$, with very large values ($AAE \sim 8$). There is a rapid, scattered decrease in the AAE as MCE increases further (Fig. 1b). The relationship between $[OA]/[BC]$ and MCE is similar, with values generally decreasing as MCE increases but with a large amount of scatter (Fig. 1d). There is also a general relationship between the mass absorption coefficient referenced to BC (MAC_{BC}) at 405 nm and the MCE , but with similar scatter to the other properties (Fig. 1c). The MAC_{BC} is defined as

$$MAC_{BC} = b_{abs}/[BC]. \quad (4)$$

The $MAC_{BC,405\text{ nm}}$ includes contributions from absorption by BC and BrC, as well as from coating-induced enhancement of BC absorption. These results, along with the literature, indicate that MCE can provide guidance as to the general magnitude of these particle properties but that the MCE is ultimately a fairly imprecise metric, especially for the $SSA_{405\text{ nm}}$.

However, we find a very strong relationship between the $SSA_{405\text{ nm}}$ and the total $[OA]/[BC]$ ratio (Fig. 1e). This is consistent with the findings of Pokhrel et al. (2016), who observed something similar but over a smaller range of $[OA]/[BC]$. (Similarly strong relationships are observed for SSA values at 532 and 781 nm (Fig. S1 in the Supplement), or if the $[NR-PM_1]/[BC]$ values are used as OA averages (95 % of the total $NR-PM_1$ mass.) Smaller $[OA]/[BC]$ values correspond to smaller $SSA_{405\text{ nm}}$ values with a sigmoidal relationship observed. (Fit parameters for all fits shown are provided in Table S1.) There is similarly a very strong, sigmoidal relationship between the AAE and $MAC_{BC,405\text{ nm}}$ and $[OA]/[BC]$ (Fig. 1f, g). The large increase in the $MAC_{BC,405\text{ nm}}$ indicates that BrC contributes substantially to the total absorption. The contributions of coating-induced enhancements and of BrC are discussed further in Sect. 3.4.1 and 3.4.2. The larger range of $[OA]/[BC]$ and the greater number of individual burns considered here, compared to Pokhrel et al. (2016), allow for the determination of more robust fits. Pokhrel et al. (2017) found that the absorption enhancement at 405 nm, determined from thermodenuder measurements, increased with $[OA]/[BC]$ up to $[OA]/[BC] \sim 33$ (the largest value reported), which is consistent with our findings.

These observations demonstrate that the optical properties of the primary particles depend on the relative amount of OA versus BC. This is as expected because OA is generally more scattering, compared to BC, and light-absorbing OA (also known as BrC) typically exhibits a much stronger wavelength dependence than BC. Based on these relationships, we divide the individual burns into different classes (Table 1). We have chosen to classify particles based on the observed $SSA_{405\text{ nm}}$ values; use of $[OA]/[BC]$ for classification yields largely similar results, given the strong relationship between the two. The dividing lines between classes are selected to yield six classes that span the entire range of $SSA_{405\text{ nm}}$ values, from 0.23 (Class 1) to 0.97 (Class 6), with approximately

equal numbers of individual burns in each class (ca. 8–10). Partitioning the observations into different particle classes facilitates the interpretation of the photochemical evolution of the particles, to be discussed in future work. In addition, we find that use of the class average properties versus MCE generally provides more representative fits to the observations (visually apparent in Fig. 1 and supported by the reduced χ^2 for the fits).


3.2 OA composition and volatility

Variability in the bulk composition of the OA is characterized by the O : C and H : C atomic ratios and the fractional abundance (f_x) of two marker ions, $m/z = 44$ and $m/z = 60$. The f_{44} is complementary to O : C and larger values generally indicate a greater degree of oxygenation and the presence of carboxylic acids. The f_{60} is often taken as a marker ion for biomass burning, in particular a signature of levoglucosan and similar molecules (Schneider et al., 2006; Alfarra et al., 2007). The high-resolution ion $C_2H_4O_2^+$ contributes to and exhibits a similar behavior to f_{60} ; the slope for $f_{C_2H_4O_2^+}$ against f_{60} is 0.98. While it is known that properties such as f_{60} vary in different biomass burning samples (Schneider et al., 2006) or between near-source intercepts of different ambient plumes (Garofalo et al., 2019), the specific dependence on burn conditions or overall particle composition (e.g., $[OA]/[BC]$) has not been systematically explored to our knowledge.

The average $f_{60} = 0.022 \pm 0.01$ (1σ). The f_{60} values vary nonmonotonically with $[OA]/[BC]$, exhibiting a slight increase from Class 1 to Class 3 and then a decrease from Class 4 to Class 6 (Fig. 2a). This indicates that, while f_{60} is overall a useful marker ion for biomass burning, it cannot be used to distinguish between different burn conditions. The f_{44} generally decreases with $[OA]/[BC]$ (Fig. 2b; $r^2 = 0.33$). However, the average f_{44} values for particle classes 2–5 differ negligibly, suggesting that f_{44} might be useful in discriminating between extreme cases (e.g., Class 1 versus Class 6) but that it is of limited general use in distinguishing between burn conditions and fuel types. The O : C atomic ratio (average = 0.37 ± 0.09) exhibits similar behavior – expected as f_{44} is generally related to O : C (Aiken et al., 2008) – with a general decrease as $[OA]/[BC]$ increases, although a comparably weaker correlation (Fig. 2c; $r^2 = 0.17$). The H : C (average = 1.76 ± 0.05) exhibits a weak, positive correlation with $[OA]/[BC]$, although the variability is slight (Fig. 2d; $r^2 = 0.27$).

The mass fraction of the OA that is composed of nitrated organics ($f_{ON-OA} = [ON]/[OA]$) was determined using the HR-ToF-AMS measurements and the method of Kiendler-Scharr et al. (2016) (see the Supplement for further details). The terminology “nitrated organics” (ON) includes contributions from both nitro and nitrate functional groups. The fraction of measured nitrate that was ON ($f_{ON-N} = [ON]/([ON] + [NO_3^-])$) decreased with $[OA]/[BC]$ and ranged from 0.91 (Class 1) to

Table 1. Fuels by particle class.

Class	Fuel	SSA range	[OA] / [BC] range
Class 1	Chaparral, canopy, litter (pine), building materials, excelsior	0.23–0.43	0.3–2.4
Class 2	Manzanita, sage, litter (fir)	0.43–0.60	1.5–4.1
Type 3	Pine, fir, litter, canopy, juniper	0.60–0.74	6.6–20
Class 4	Pine, fir, canopy, rotten log, ceonothos 	0.74–0.87	8.3–55
Class 5	Canopy (pine), rice, bear grass, duff	0.87–0.93	31–143
Class 6	Rotten log, duff, peat, dung	0.93–1.00	431–10 ⁵

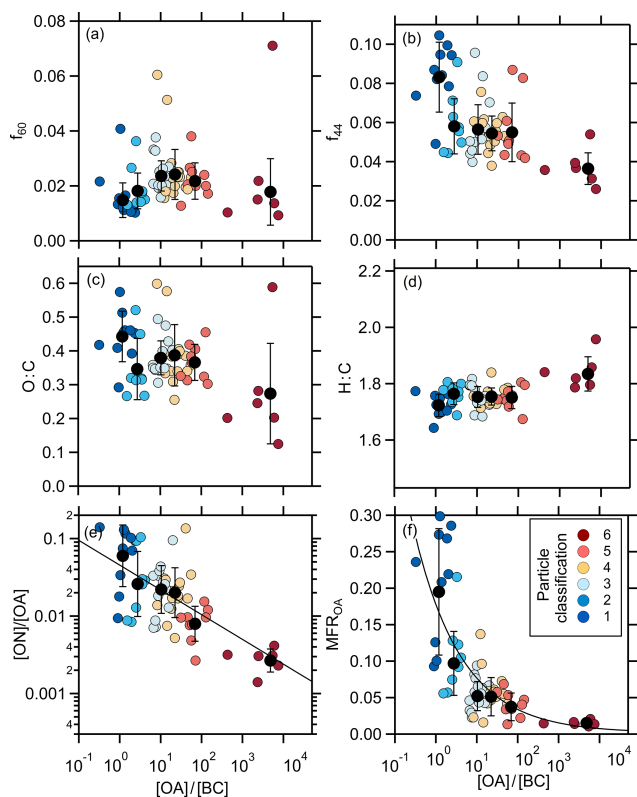


Figure 2. Dependence of (a) f_{60} ; (b) f_{44} ; (c) O:C; (d) H:C; (e) the nitrated organic fraction of OA, $f_{\text{ON-OA}}$; and (f) the OA volatility, characterized as the mass fraction remaining after heating. Results for individual burns are shown as points colored by the particle class, and class average values are shown as black circles. Uncertainties on the class averages are 1σ based on measurement variability. For $f_{\text{ON-OA}}$ and MFR_{OA} , fits to the observations are shown (see text).

0.48 (Class 6) (Fig. S2a). The class-specific average $f_{\text{ON-OA}}$ also decreased with $[\text{OA}] / [\text{BC}]$, although by a much greater extent than the $f_{\text{ON-N}}$, ranging from 6.0 % (Class 1) to 0.27 % (Class 6) and (Fig. 2e). There is a reasonably linear relationship between $\log(f_{\text{ON-OA}})$ and $\log([\text{OA}] / [\text{BC}])$ ($r^2 = 0.47$). This indicates that a larger proportion of ON species and functionalities are produced when particles are, on average, more BC-rich. This does not reflect differences in

fuel nitrogen content as there is no relationship between fuel N and $f_{\text{ON-OA}}$ (Fig. S2b). Therefore, it seems that the relationship between $f_{\text{ON-OA}}$ and $[\text{OA}] / [\text{BC}]$ is related more so to the burn conditions than the fuel N content, although as with many other properties the relationship with $[\text{OA}] / [\text{BC}]$ is clearer than with the MCE (Fig. S2c).

The OA volatility is characterized as the ratio between the OA concentration after thermodenuding to that without thermodenuding (the mass fraction remaining, MFR_{OA}). The MFR_{OA} decreases as $[\text{OA}] / [\text{BC}]$ increases (Fig. 2f), indicating that the OA at lower $[\text{OA}] / [\text{BC}]$ values is less volatile than the OA at higher values. This observation provides support for the proposal by Saleh et al. (2014) that less volatile, more absorbing species are preferentially formed under conditions where BC formation is favored, which is discussed further in Sect. 3.4.2. The relationship between MFR_{OA} and $[\text{OA}] / [\text{BC}]$ is reasonably described by an exponential function.

3.3 BC nixing state

As discussed above, the relative amounts of OA and BC vary greatly between fuel types and combustion conditions. However, the distribution of BC and OA between particles, and how this varies between very different burn conditions, has not been previously explored in detail to our knowledge. The bulk average fraction of OA that is internally mixed with BC versus OA that is externally mixed from BC is determined using the HR-ToF-AMS and SP-AMS measurements. The HR-ToF-AMS quantifies OA independent of mixing state, whereas the SP-AMS (as operated here) quantifies only the OA that is internally mixed with BC. The fraction of OA that is internally mixed with BC ($f_{\text{OA,int}}$) is

$$f_{\text{OA,int}} = \frac{[\text{OA}]_{\text{SP-AMS}}}{[\text{OA}]_{\text{HR-ToF-AMS}}} = \frac{[\text{OA}]_{\text{int}}}{[\text{OA}]_{\text{tot}}}, \quad (5)$$

where the subscript int indicates the OA that is internally mixed with BC and the subscript tot indicates the total OA. The $f_{\text{OA,int}}$ should range from 0 to 1. Related, the SP-AMS quantified the ratio between the OA that is internally mixed with BC and the BC concentration, referred to here as $[\text{OA}]_{\text{int}} / [\text{BC}]$. We find that $f_{\text{OA,int}}$ decreases substantially as $[\text{OA}] / [\text{BC}]$ increases, ranging from $f_{\text{OA,int}} = 0.4$ for Class 1 (low SSA) particles to $f_{\text{OA,int}} = 0.01$ for Class

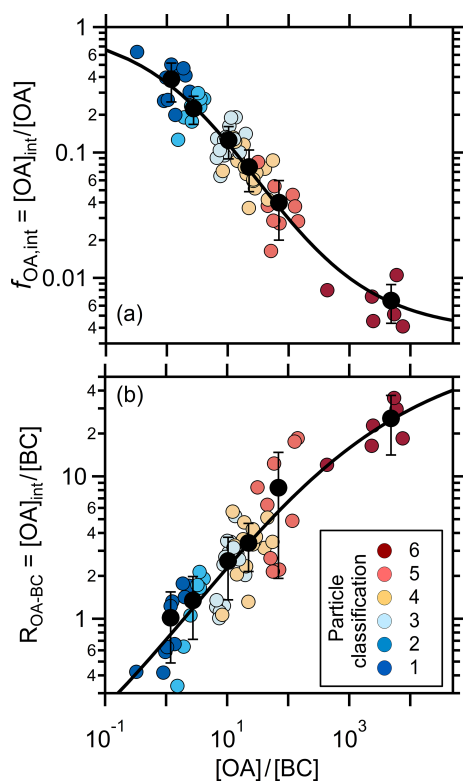


Figure 3. Relationship between the total $[OA]/[BC]$ mass ratio and (a) the fraction of OA that is internally mixed with BC, $f_{OA,int}$; and (b) the OA-to-BC mass ratio for only the internally mixed OA. Results for individual burns are shown as points colored by the particle class, and class average values are shown as black circles. Uncertainties on the class averages are 1σ based on measurement variability. Black lines are sigmoidal fits to the data, in log–log space.

6 (high SSA) particles (Fig. 3a). The data are well-fit by a sigmoidal function. However, the amount of OA coating BC ($R_{OA-BC} = [OA]_{int}/[BC]$) increases with the total $[OA]/[BC]$, also with a sigmoidal relationship (Fig. 3b). Thus, while a smaller fraction of the total OA is internally mixed with BC for larger total $[OA]/[BC]$, the amount of OA that coats BC increases. Most likely, this behavior reflects the fact that BC and OA are generated with different efficiencies in different parts of the combusting biomass. BC is more efficiently generated from flaming combustion, while OA is more efficiently generated from smoldering combustion. These observations demonstrate that the extent to which atmospheric models can assume that all OA is internally mixed with or externally mixed from BC at the point of emission will depend on the combustion conditions.

3.4 Absorption enhancement and brown carbon

3.4.1 Coating-induced absorption enhancement

Non- or weakly absorbing coatings on black carbon particles can theoretically increase the absorption by BC (Fuller et al., 1999; Bond et al., 2006), an effect which has been confirmed by laboratory experiments (Lack et al., 2009; Shiraiwa et al., 2010; Cappa et al., 2012). The extent to which coatings on BC actually enhance absorption by BC in the atmosphere remains unclear. Some studies indicate minor coating-induced enhancements while others indicate substantial enhancements (Cappa et al., 2012, 2019b; Healy et al., 2015; Liu et al., 2015, 2017; Peng et al., 2016; Zhang et al., 2016). Understanding the nature of the coating-induced enhancement is important for quantifying the radiative impacts of BC (Jacobson, 2001; Bond et al., 2013). Further, these coating-induced absorption enhancements ($E_{abs,coat}$) complicate the determination of brown carbon (BrC) absorption, and the two must be separated. Here, we examine the extent to which coatings on BC for primary biomass burning particles enhance the BC absorption. Theoretically, the magnitude of $E_{abs,coat}$ for an individual particle depends primarily on the coating thickness and secondarily on the size of the BC core (Bond et al., 2006; Fuller et al., 1999). Thus, the extent to which coatings enhance BC absorption for a given situation can be assessed through the relationship between the observed MAC_{BC} and the coating-to-core mass ratio ($R_{coat-rBC} = [NR-PM]_{int}/[BC]$, where int indicates that the coating material is internally mixed with BC). The expectation is that the MAC_{BC} increases with $R_{coat-rBC}$.

However, absorption by BrC can also lead to an apparent increase in the normalized absorption with R_{BC} if the BrC abundance correlates with the total coating amount. Because BrC absorbs more strongly at shorter wavelengths, the wavelength dependence of the MAC_{BC} -to- R_{BC} relationship can be used to further separate the influence of coating versus BrC absorption. The MAC_{BC} exhibits a wavelength-dependent relationship with $R_{coat-rBC}$ for fresh biomass particles (405, 532, and 781 nm) (Fig. 4a–c). The MAC_{BC} increases notably with $R_{coat-rBC}$ at 405 nm and to a lesser extent at 532 nm. At 781 nm the MAC_{BC} is essentially independent of $R_{coat-rBC}$ up to $R_{coat-rBC}$ values as large as 10 but does exhibit some increase at $R_{coat-rBC} > 10$. However, this is most likely a result of absorption by OA at 781 nm and not indicative of an increase in the coating-induced enhancement, discussed further below. The wavelength dependence provides clear evidence of BrC absorption at shorter wavelengths.

That the MAC_{BC} at 781 nm is nearly independent of $R_{coat-rBC}$ up to such large $R_{coat-rBC}$ values indicates that there is only a minor coating-induced enhancement for the primary biomass particles, the magnitude of which is discussed below. Our observations are consistent with McMeeking et al. (2014), who also investigated the relationship between the MAC_{BC} and $R_{coat-rBC}$ for primary biomass particles from

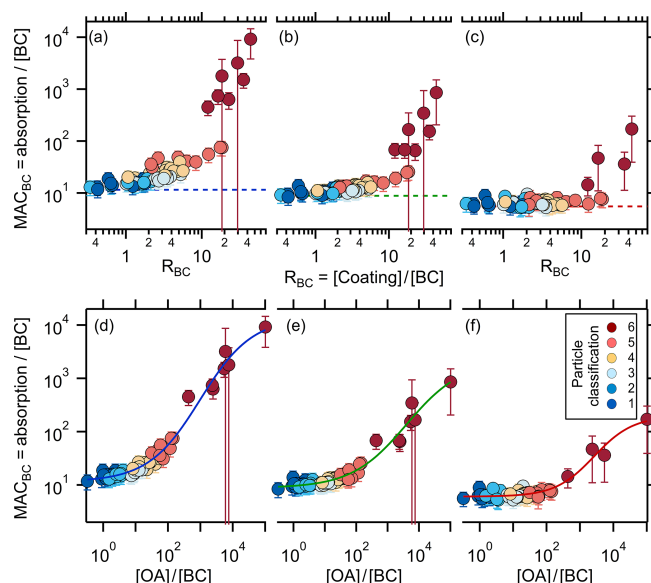


Figure 4. (a–c) The relationship between the wavelength-specific MAC_{BC} and the coating-to-BC mass ratio for (a) 405 nm, (b) 532 nm, and (c) 781 nm. The horizontal dashed lines show the derived $\text{MAC}_{\text{BC,pure}}$ values. (d–f) The relationship between the wavelength-dependent MAC_{BC} and the total $[\text{OA}]/[\text{BC}]$ mass ratio for (d) 405 nm, (e) 532 nm, and (f) 781 nm. The lines are sigmoidal fits. Uncertainties for the individual burns are determined from error propagation. Graphs of the wavelength-specific MAC_{BC} versus $[\text{OA}]/[\text{BC}]$ with each shown using independent y-axis scales are provided for comparison in Fig. S1.

multiple fuel types. Most likely, this lack of a substantial coating-induced enhancement results from a noneven distribution of non-BC mass across the population of BC particles (Fierce et al., 2016; Liu et al., 2017) and from the morphology of BC-containing particles not conforming to an idealized core-shell structure (Adachi et al., 2010). The influence of photochemical aging on the coating-induced enhancement will be examined in future work.

The relationship between MAC_{BC} and the coating amount ($R_{\text{coat-rBC}}$) can be contrasted with the relationship between MAC_{BC} and the total $[\text{OA}]/[\text{BC}]$. At all three wavelengths the MAC_{BC} 's exhibit strong, sigmoidal relationships with $[\text{OA}]/[\text{BC}]$ (Fig. 4d–f). That $\text{MAC}_{\text{BC,781 nm}}$ exhibits such a clear relationship with $[\text{OA}]/[\text{BC}]$ suggests that even the small, apparent coating-induced enhancement, implied above from the very weak with $R_{\text{coat-rBC}}$, is largely driven by absorption by BrC rather than from the impact of coating on BC. Pokhrel et al. (2017) found that the absorption enhancement, determined from thermodenuder measurements, increased notably with $[\text{OA}]/[\text{BC}]$ up to $[\text{OA}]/[\text{BC}] \sim 33$ at 405 nm (the largest value reported by them) but by much less at 660 nm, which is consistent with our findings.

The observations allow for determination of wavelength-dependent MAC_{BC} values for pure BC ($\text{MAC}_{\text{BC,pure}}$) for each wavelength by extrapolation of the MAC_{BC} versus

$[\text{OA}]/[\text{BC}]$ ratio to zero using sigmoid fits. Since the $R_{\text{coat-rBC}}$ correlates reasonably with $[\text{OA}]/[\text{BC}]$ (Fig. 3b), extrapolation against $[\text{OA}]/[\text{BC}]$ to zero effectively removes both contributions from BrC and any coating-induced enhancement. The derived $\text{MAC}_{\text{BC,pure}}$ values are $11.8 \text{ m}^2 \text{ g}^{-1}$ at 405 nm, $8.8 \text{ m}^2 \text{ g}^{-1}$ at 532 nm, and $5.5 \text{ m}^2 \text{ g}^{-1}$ at 781 nm, with estimated fit-based uncertainties of $\sim 10\%$. The absolute uncertainties on the $\text{MAC}_{\text{BC,pure}}$ are primarily dependent on the uncertainty in the b_{abs} and $[\text{rBC}]$ measurements and are $\sim 35\%$. The derived MAC_{BC} values are very similar to those recently reported by Forestieri et al. (2018) for fresh BC particles: $\text{MAC}_{\text{BC,pure}} = 11.9 \text{ m}^2 \text{ g}^{-1}$ at 405 nm and $8.8 \text{ m}^2 \text{ g}^{-1}$ at 532 nm, with an extrapolated value at 781 nm of $5.7 \text{ m}^2 \text{ g}^{-1}$. The value at 532 nm is somewhat higher than that suggested by Bond and Bergstrom (2006) ($7.75 \text{ m}^2 \text{ g}^{-1}$ at 532 nm). Our derived $\text{MAC}_{\text{BC,pure}}$ values yield an AAE = 1.17, determined from a fit to the three wavelengths. An AAE close to unity indicates absorption is dominated by BC, as expected.

Values for the absorption enhancement at 781 nm are calculated as the ratio between the observed MAC_{BC} in Fig. 4 and the derived $\text{MAC}_{\text{BC,pure}}$. The derived E_{abs} values range from 0.96 to 27. Values greater than 2 occur only for the particles having particularly large $[\text{OA}]/[\text{BC}]$, > 400 . As E_{abs} values much greater than 2 at 781 nm are unlikely to result from mixing-induced enhancements (Chakrabarty and Heinson, 2018), this again suggests that the OA is somewhat absorbing at this wavelength. For the burns where $[\text{OA}]/[\text{BC}] < 400$, the median $E_{\text{abs}} = 1.14$ and the arithmetic mean $E_{\text{abs}} = 1.19 \pm 0.14 (1\sigma)$. Given that some of this enhancement may result from BrC absorption at 781, these values can be considered upper limits on $E_{\text{abs,coat}}$, and the small magnitude is consistent with our conclusion above that, while likely greater than 0, the mixing-induced enhancement is generally minor. It is possible that the $E_{\text{abs,coat}}$ values when $[\text{OA}]/[\text{BC}] > 400$ are substantially larger. However, given the general lack of a dependence of the $\text{MAC}_{\text{BC,781 nm}}$ for $R_{\text{BC-coat}} < 10$, this seems unlikely.

3.4.2 Primary brown carbon absorption

The absorption due to brown carbon is determined by the difference as

$$b_{\text{abs,BrC}} = b_{\text{abs,obs}} - \text{MAC}_{\text{BC,pure}} \cdot [\text{BC}] \cdot E_{\text{abs,coat}}, \quad (6)$$

where $b_{\text{abs,BrC}}$ is the absorption due to BrC specifically. Importantly, the use of study-specific $\text{MAC}_{\text{BC,pure}}$ values serves to reduce systematic biases in the $b_{\text{abs,BrC}}$, compared to direct use of literature $\text{MAC}_{\text{BC,pure}}$ values. Assuming $E_{\text{abs,coat}} = 1$ provides an upper limit on the BrC absorption, which we note is likely most appropriate for the particles sampled here, as discussed in the previous section. Therefore, we use the upper-limit values throughout the analysis that follows, unless otherwise stated. However, a lower limit for BrC absorption can be determined

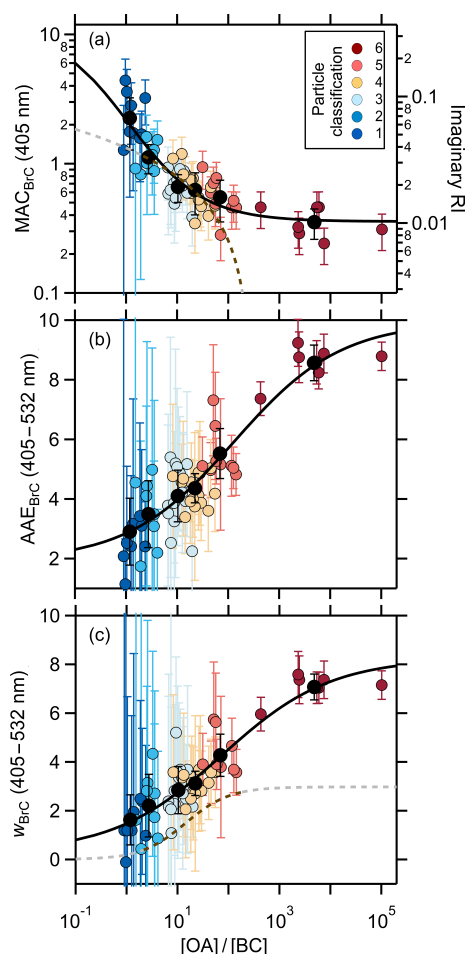


Figure 5. Relationship between (a) $\text{MAC}_{\text{BrC},405 \text{ nm}}$, (b) $\text{AAE}_{\text{BrC},405-532}$, and (c) $w_{\text{BrC},405-532}$ and the $[\text{OA}]/[\text{BC}]$ mass ratio. The solid lines are sigmoidal fits to the observations against $\log([\text{OA}]/[\text{BC}])$. The dashed lines are based on the parameterization of Saleh et al. (2014), with the brown color indicating the measuring range in that study and the gray color extrapolated. Results for individual burns are shown as points colored by the particle class, and class average values are shown as black circles. Uncertainties on the class averages are 1σ based on measurement variability. Uncertainties for the individual burns are determined from error propagation.

at 405 and 532 nm assuming that all of the enhancement at 781 nm results from coatings and not from BrC. The resulting $E_{\text{abs,obs}} (= \text{MAC}_{\text{BC,obs}}/\text{MAC}_{\text{BC,pure}})$ at 781 nm averages 1.19 for $R_{\text{BC-coat}} < 10$. Using $E_{\text{abs,coat}} = 1.19$ in Eq. (7) yields a lower limit for the BrC absorption at the two shorter wavelengths, which is appropriate since $E_{\text{abs,coat}}$ generally has only a small wavelength dependence. A fit to the coating-corrected (lower-limit) versus upper-limit $b_{\text{abs,BrC}}$ yields a slope of 0.97 at 405 nm and 0.88 at 532 nm (Fig. S3). The smaller difference at 405 nm results from the fractional contribution of BrC to the total absorption being larger at this wavelength.

Brown-carbon-specific mass absorption coefficients (MAC_{BrC}) are determined as the ratio between $b_{\text{abs,BrC}}$ and the total OA concentration:

$$\text{MAC}_{\text{BrC}} = \frac{b_{\text{abs,BrC}}}{[\text{OA}]} \quad (7)$$

The MAC_{BrC} values from Eq. (7) are bulk average values and do not account for different molecules and classes of molecules likely having different absorptivities. Uncertainties in the MAC_{BrC} values are determined by error propagation. Similarly, an AAE value for just the brown carbon (AAE_{BrC}) can be calculated using wavelength pairs as

$$\text{AAE}_{\text{BrC}} = -\log\left(\frac{b_{\text{abs,BrC},\lambda_1}}{b_{\text{abs,BrC},\lambda_2}}\right) / \log\left(\frac{\lambda_1}{\lambda_2}\right) \quad (8)$$

The geometric averages of the MAC_{BrC} values are $0.76^{+0.65}_{-0.35}$, $0.21^{+0.36}_{-0.13}$, and $0.056^{+0.15}_{-0.04} \text{ m}^2 \text{ g}^{-1}$ at 405, 532, and 781 nm, with uncertainties the 1σ burn-to-burn variability. The MAC_{BrC} values vary between classes, generally increasing as the $[\text{OA}]/[\text{BC}]$ ratio decreases at all wavelengths (shown for 405 nm in Fig. 5a). For example, the average $\text{MAC}_{405 \text{ nm}} = 2.3 \pm 1 \text{ m}^2 \text{ g}^{-1}$ for Class 1 and $0.35 \pm 0.09 \text{ m}^2 \text{ g}^{-1}$ for Class 6. Although the uncertainties on the derived MAC_{BrC} increase substantially as $[\text{OA}]/[\text{BC}]$ decreases – because BrC absorption contributes to a smaller extent at longer wavelengths – the observations nonetheless indicate that the BrC absorptivity depends on the combustion conditions. The relationship at 405 nm is well-described by a sigmoidal function in log–log space, with limiting values of $0.35 \text{ m}^2 \text{ g}^{-1}$ at large $[\text{OA}]/[\text{BC}]$ and $11.2 \text{ m}^2 \text{ g}^{-1}$ at small $[\text{OA}]/[\text{BC}]$. That the extrapolated zero $[\text{OA}]/[\text{BC}]$ limit for MAC_{BrC} is similar to pure BC suggests an evolution of BrC towards having properties similar to BC when the overall $[\text{OA}]$ content is small. Such behavior is consistent with Saleh et al. (2018), who argue that there is a continuum of BrC properties that depends on the combustion conditions, as demonstrated in that study for low-temperature benzene and toluene combustion. The range of the MAC_{BrC} values observed here, including that there is notable absorption at 781 nm, encompass many previous measurements, summarized in Table S3. This likely reflects the wide diversity of fuel types and burn conditions considered here, as exemplified by the very large range of $[\text{OA}]/[\text{BC}]$.

Estimated values of the imaginary component of the refractive index for BrC (k_{BrC}) are determined from Mie theory via optical closure (Zhang et al., 2016), assuming a real part of the refractive index of 1.5 and a particle diameter of 150 nm, a typical value for these experiments. Imaginary RI_{BrC} values are of use in atmospheric models for calculation of BrC absorption. There is a linear relationship between MAC_{BrC} and k_{BrC} (Fig. S4a). Thus, the k_{BrC} exhibits a similar correlation with $[\text{OA}]/[\text{BC}]$ as does the MAC_{BrC} (Fig. 5a).

The wavelength dependence of absorption, i.e., the $\text{AAE}_{405-532}$, also varies with $[\text{OA}]/[\text{BC}]$, in this case with

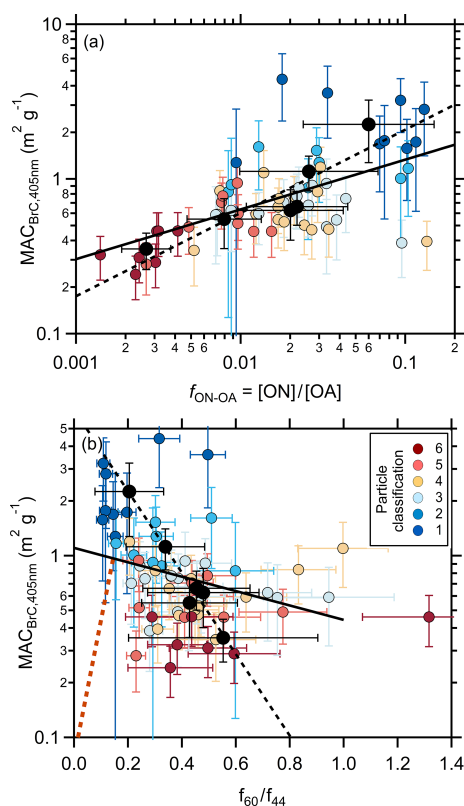


Figure 6. Relationship between the $\text{MAC}_{\text{BrC},405\text{ nm}}$ and (a) the nitrated organic fraction of total organic aerosol, $f_{\text{ON-OA}}$, and (b) the f_{60}/f_{44} ion ratio for organic aerosol. Results for individual burns are shown as points colored by the particle class, and class average values are shown as black circles. Uncertainties on the class averages are 1σ based on measurement variability. Uncertainties for the individual burns are determined from error propagation. Solid black lines are fits to all burns and dashed black lines are fits to the class averages. The dashed brown line in (b) is the relationship reported by Lack et al. (2013) for ambient particles in a biomass burning plume.

a positive relationship between the two (Fig. 5b). The relationship is reasonably described by a sigmoidal function. This implies that, while the MAC_{BrC} varies inversely with $[\text{OA}]/[\text{BC}]$ at all wavelengths, the exact variation is wavelength dependent. The $\text{AAE}_{405-532}$ relationship with $[\text{OA}]/[\text{BC}]$ is well-described by a sigmoidal function (versus $\log([\text{OA}]/[\text{BC}])$), with limiting values of 10.4 at large $[\text{OA}]/[\text{BC}]$ and 1.3 at small $[\text{OA}]/[\text{BC}]$. The wavelength dependence of the k_{BrC} (w_{BrC}) are also calculated, to facilitate comparison with the literature, as

$$w_{\text{BrC}} = -\log\left(\frac{k_{\text{BrC},\lambda 1}}{k_{\text{BrC},\lambda 2}}\right) / \log\left(\frac{\lambda 1}{\lambda 2}\right). \quad (9)$$

The w_{BrC} 's exhibit a similar dependence on $[\text{OA}]/[\text{BC}]$ as the AAE_{BrC} , as the w_{BrC} and AAE_{BrC} are linearly related, albeit with some scatter (Fig. S4b; $r^2 = 0.97$).

Our observations support the results of Saleh et al. (2014), who also found a relationship between the $k_{\text{BrC},405\text{ nm}}$ and $[\text{OA}]/[\text{BC}]$. However, our analysis substantially extends the range of $[\text{OA}]/[\text{BC}]$ values investigated in that work (they considered $[\text{OA}]/[\text{BC}]$ from only ca. 2 to 170). In the overlap region between our two studies the $k_{\text{BrC},405\text{ nm}}$ values agree reasonably well over the range $2 < [\text{OA}]/[\text{BC}] < 50$, but the $k_{\text{BrC},405\text{ nm}}$ values from Saleh et al. (2014) are smaller than observed here above $[\text{OA}]/[\text{BC}] = 50$. Importantly, our results demonstrate that the linear fit suggested by Saleh et al. (2014) for MAC_{BrC} is only appropriate over the range of values they considered and that a sigmoidal fit provides for a more robust relationship over a wider range of $[\text{OA}]/[\text{BC}]$. Related, the wider range of $[\text{OA}]/[\text{BC}]$ enables more robust determination of the functional dependence of the wavelength dependence of absorption (w_{BrC}), with overall larger w_{BrC} values and a larger plateau at high $[\text{OA}]/[\text{BC}]$ compared to the fit by Saleh et al. (2014).

The MAC_{BrC} values also correlate with the nitrated organic fraction of OA, the latter of which, as noted above, also correlates with the $[\text{OA}]/[\text{BC}]$ (Fig. 6a). This observation suggests that organic nitrate and nitro functionalities may be at least somewhat responsible for the increase in absorption. Laskin et al. (2018) performed offline molecular level analyses of primary OA collected during FIREX. They found that nitroaromatics and N-containing polycyclic aromatic hydrocarbons (PAHs) contribute notably to the total light absorption by BrC, although there are many non-N-containing species that also contribute to BrC absorption. The variability between particle classes is consistent with the results of Lin et al. (2016), which show that the abundance of N-containing chromophores varies between particles produced from different biomass fuels. Additionally, Mohr et al. (2013) observed a relationship between the concentration of nitrated phenols and short-wavelength absorption by BrC, although it is possible that for their measurements these species were produced from chemical processing, as opposed to being directly emitted. Altogether, our results provide support for the idea that nitrated organic functionalities are an important contributor to BrC absorption. However, it is very likely that other functional groups also contribute to the total absorption.

The $\text{MAC}_{\text{BrC},405\text{ nm}}$ exhibits an inverse correlation with the f_{60}/f_{44} ratio of the OA, although there is substantial scatter in the f_{60}/f_{44} ratio for a given particle class (Fig. 6b). (The f_{44} and f_{60} have no discernable relationship.) The observed $\text{MAC}_{\text{BrC},405\text{ nm}}$ relationship with f_{60}/f_{44} is opposite that reported by Lack et al. (2013) for ambient measurements of particles of a biomass burning plume, and they found a reasonable positive correlation. This difference in behavior results from our sampling primary particles directly – thereby focusing on the inherent variability in the properties of the emitted particles – while Lack et al. (2013) sampled ambient particles. For ambient sampling, the observed relationship will be sensitive to mixing of biomass burning particles with background or aged biomass particles, which are known

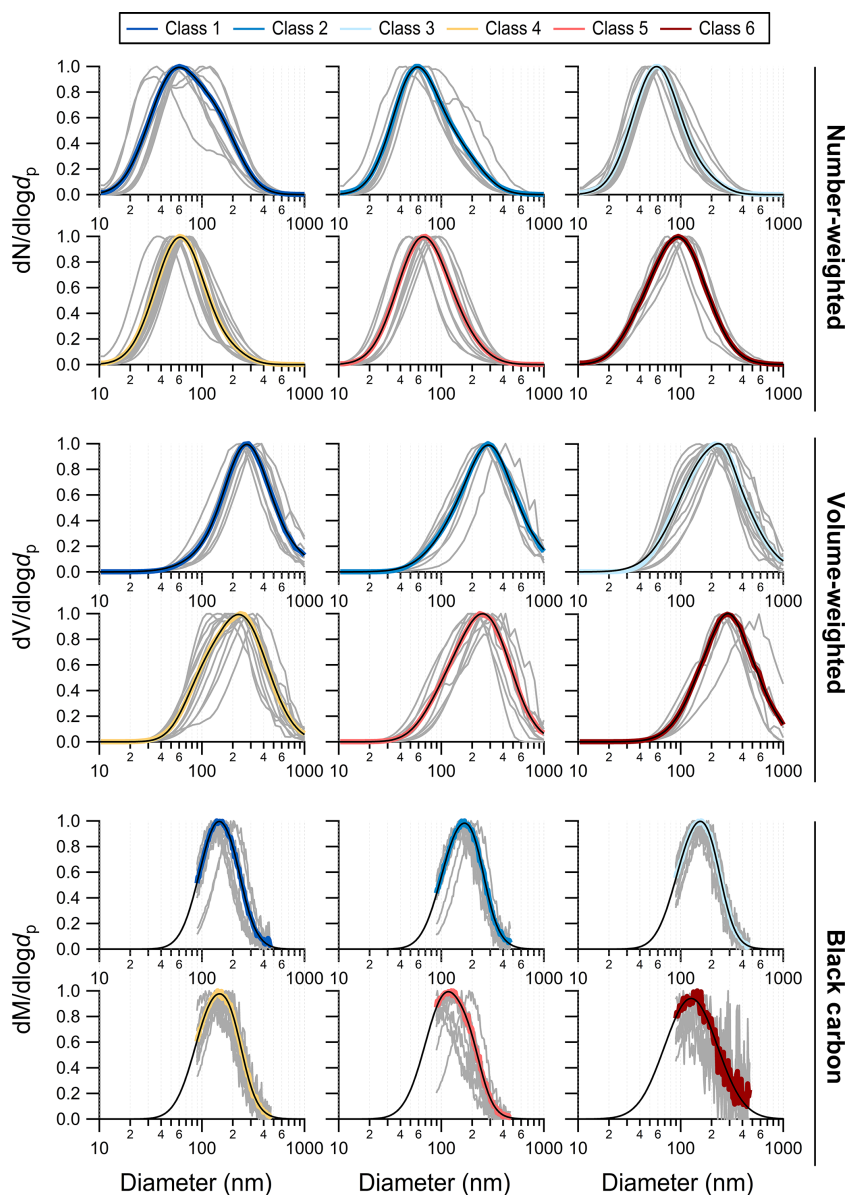


Figure 7. Class-specific total particle number-weighted (top) and volume-weighted (middle) mobility size distributions, and the BC-only mass-weighted (bottom) size distribution. Individual burns are shown in gray and class averages are shown as colors. Bimodal lognormal fits are thin black lines. Note that the number-weighted and volume-weighted distributions are graphed versus mobility diameter and the BC mass-weighted distribution against the BC volume equivalent diameter.

to have a smaller f_{60} . (Cubison et al., 2011). Thus, the relationship observed by Lack et al. (2013) can best be viewed as a mixing line between the fresh primary particles (having large $\text{MAC}_{\text{BrC},405 \text{ nm}}$ and large f_{60}/f_{44}) and background or aged biomass particles (having small $\text{MAC}_{\text{BrC},405 \text{ nm}}$ and small f_{60}/f_{44}), rather than providing information on the inherent variability in the absorptivity of the fresh particles.

3.5 Size distributions

Total particle mobility size distributions and BC-only size distributions were measured (Fig. 7). Primary particle size distributions are important parameters specified in regional and global models. The number-weighted and volume-weighted size distribution are generally described by either one or two lognormal modes for individual burns; a two-mode fit provides a more robust solution across all modes. The mass-weighted BC size distributions are similarly described by one or two lognormal modes. A fit to the aver-

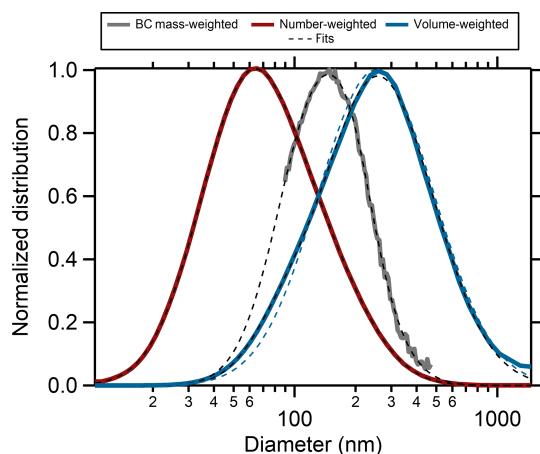


Figure 8. Average total particle number-weighted (red) and volume-weighted (blue) size distributions and the BC-specific mass-weighted size distributions. Black dashed lines are bimodal lognormal fits. The dashed blue line is the total particle volume-weighted distribution calculated from a single-mode fit to the number-weighted distribution. Note that the number-weighted and volume-weighted distributions are graphed versus mobility diameter and the BC mass-weighted distribution against the BC volume equivalent diameter.

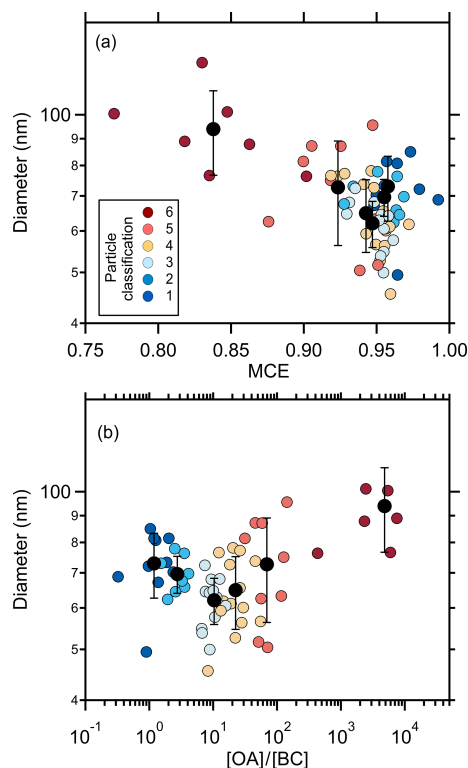


Figure 9. Relationship between number-weighted particle median diameter and (a) the MCE and (b) the $[OA]/[BC]$ ratio. Colored circles are for individual burns and black circles for particle class averages.

age number-weighted distribution across all particle classes yields geometric median diameters ($d_{p,N}$) and widths (σ_g) of 60.3 and 1.76 nm^{TS6}, respectively, for the smaller mode and 153 nm and 1.64 for the larger mode (Fig. 8). The amplitude of the smaller mode is 4.6 times the larger mode. A single-mode fit yields $d_{p,N} = 68$ nm and $\chi_g = 1.93$, although the fit is poorer. Mann et al. (2014) report $d_{p,N}$ values used by a variety of global models for biofuels. The models tend to use either 80 nm or 150 nm, although a few use other values (30, 60, 100 nm). Those using 80 nm typically use $\sigma_g = 1.80$ while those using 150 nm typically use $\sigma_g = 1.59$, although there are exceptions. Our observations indicate that use of a bimodal distribution within models would be more representative, but that a single mode can perform acceptably. We find that the volume-weighted distribution calculated from a single-mode fit to the number-weighted distribution is similar to the observed volume-weighted distribution (Fig. 8). Thus, the use of a single mode to represent biomass burning size distributions thus appears acceptable, so long as the appropriate parameters are used. In this context, the widths of the distribution used by the various global models appear somewhat too small. However, we note that the microphysics occurring in the fresh smoke sampled here, which will govern the size distributions, may differ from that in atmospheric plumes.

The average BC-specific mass-weighted size distribution mode is at 148 nm (Fig. 8). A bimodal fit yields values for the mass median diameter ($d_{p,M}$) as well as σ_g of 137.2 and 1.62 nm^{TS7}, respectively, for the smaller mode and 197.1 nm

and 1.24 for the larger mode, with most of the mass contained in the smaller mode. May et al. (2014) report $d_{p,M}$ from laboratory biomass combustion ranging from 140 to 190 nm, averaging 170 nm. Their average is somewhat larger than ours, likely reflecting differences in the exact fuels sampled. The mode diameter for the BC-specific distribution is especially smaller than observed for biomass burning particles from some ambient observations, which tend to give values closer to 200 nm (Schwarz et al., 2008; Kondo et al., 2011; Sahu et al., 2012; May et al., 2014; Cappa et al., 2019b). This difference between lab and field observations was also noted by May et al. (2014). We speculate that the influence of coagulation may be suppressed in our experiments relative to what occurs in the atmosphere due to slower overall dilution, leading to smaller BC size distributions. To the extent this is the reason for the difference, the total particle distributions would also be biased towards particles that are too small compared to the atmosphere. However, there is no relationship between $d_{p,N}$ and the total particle number concentration for our experiments. Formation of secondary aerosol in the near-field of a sampled ambient plume could also contribute to this difference.

There is substantial variability between individual burns within a given particle class in terms of the shape of the

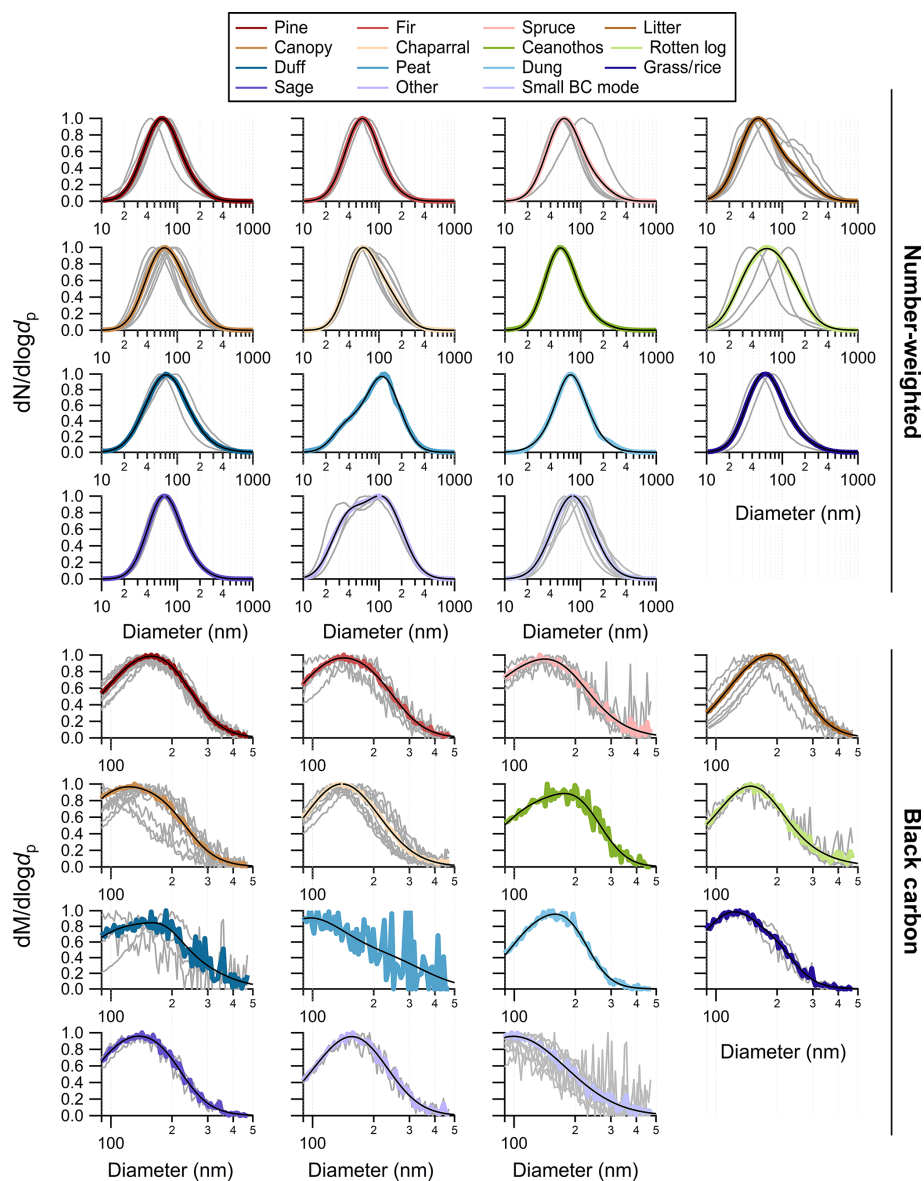


Figure 10. Normalized total particle number-weighted (top) and the BC-only mass-weighted (bottom) size distributions shown by fuel type (see legend). Individual burns are gray and averages for a fuel type in color. For some fuels there is only one size distribution. Bimodal lognormal fits are the black lines. The “other” category includes nontraditional biofuels, specifically building materials and excelsior.

size distributions (Fig. 7). This variability is most evident for Class 1, 2, and 5 but present for all classes. Nonetheless, the number-weighted mean diameter ($d_{p,N,\text{mean}}$) appears to decrease somewhat with MCE (Fig. 9; $r^2 = 0.38$). However, the relationship is largely driven by the Class 6 particles, which generally have lower MCE values, having larger $d_{p,N,\text{mean}}$ values. A lack of any particularly clear relationship is consistent with Hosseini et al. (2010), who observed the $d_{p,N,\text{mean}}$ to exhibit a complex relationship with combustion conditions. The $d_{p,N,\text{mean}}$ varies nonmonotonically with $[\text{OA}] / [\text{BC}]$, with particle size first decreasing slightly as $[\text{OA}] / [\text{BC}]$ increases (from Class 1 to Class 3) and then

increasing with further increases in $[\text{OA}] / [\text{BC}]$ (from Class 4 to Class 6) (Fig. 9). This is despite the notable burn-to-burn variability. It is important to note that the mobility-based size is particle shape dependent; very-BC-rich particles are more likely to have nonspherical shapes and thus have larger mobility diameters. This could explain the minimum in $d_{p,N}$ around Class 3 particles, for which $[\text{OA}] / [\text{BC}] = 10$.

Some of the variability within a class appears related to the presence of different fuel types within a class. Number-weighted and BC-specific mass-weighted size distributions by fuel type are shown in Fig. 10. For the number-weighted distributions, leaf litter and rotten logs exhibit the greatest

variability between different burns, although we note that multiple burns were not performed for all fuels. The shapes of the leaf litter, peat and “other” fuel types, differ most notably from the other fuel types, with the presence of more than one mode more apparent. (The “other” category here includes nontraditional biofuels, specifically building materials and excelsior.) For the BC-specific size distributions, the litter, canopy, and duff exhibited the greatest intrafuel variability. For most fuels, the BC-specific distribution peaks around 150 nm, as noted above. However, for a subset of burns (eight of them) the BC-specific distribution peaks around 100 nm (Fig. 10). These small BC-mode distributions occur for the OA-rich particle classes 4, 5 and 6 (Fig. 7), although there is no clear pattern to their occurrence.

4 Conclusions and implications

Measurements of primary particles produced from combustion of a variety of biomass fuel types indicate the optical, physical, and chemical properties of the emitted particles exhibit wide variability. We show that variability in many optical properties (e.g., single-scatter albedo, wavelength dependence of absorption, mass absorptivity of black and brown carbon) is directly linked to the [OA] / [BC] ratio of the emitted particles; the relationships with [OA] / [BC] are much stronger than with the commonly used modified combustion efficiency, and mathematical relationships between the various properties are determined. However, the absorption enhancement due to coating of BC (the so-called lensing effect) is shown to be minor and essentially independent of the amount of coating up to large coating-to-BC mass ratios. The brown carbon mass absorptivity correlates with the nitrated organic fraction of OA, suggesting that nitrated organic species contribute to BrC absorption. Many bulk chemical properties (i.e., O : C, H : C, and the relative concentrations of key marker ions such as f_{60}) exhibit limited dependence on the burn conditions and the [OA] / [BC] ratio. However, both the OA volatility and nitrated organic fraction of OA decrease with [OA] / [BC]. The fraction of OA that is internally mixed with BC was shown to decrease strongly with the [OA] / [BC] ratio, from nearly all OA being internally mixed with BC when the particles are overall BC-rich to only a few percent of OA being mixed with BC when OA dominates. Yet, the relative amount of OA coating the BC increases with [OA] / [BC]; that is, when more of the OA is externally mixed from BC those particles that do contain BC nonetheless have thicker OA coatings. The observed total particle size distributions are reasonably well described by a single lognormal mode but are better fit using a bimodal distribution. The BC-specific size distributions are similarly best fit using a bimodal distribution, although a single mode provides a reasonable representation. The dependence of the geometric median mobility diameter on the burn conditions or particle state (i.e., the [OA] / [BC]) is complicated by the mo-

bility diameter being sensitive to variations in particle shape, which depend on the [OA] / [BC] ratio. Overall, these results expand on previous observations of primary biomass burning particle properties, considering a wider range of [OA] / [BC] and associated properties. Further, they provide a foundation for understanding the postemission evolution of biomass burning smoke due to photochemical oxidation as discussed in Lim et al. (2019).

Data availability. All data are available from the NOAA FIREX-AQ data repository (<https://esrl.noaa.gov/csd/projects/firex/firelab/>TS8). This includes a summary of the fuel types used for each burn and the measurement time series for each burn. The primary particle averages used in this work are additionally collected in the UC DASH data repository (Cappa et al., 2019a).

Supplement. The supplement related to this article is available online at: <https://doi.org/10.5194/acp-20-1-2020-supplement>.

Author contributions. CDC and JHK designed the experiments. CDC, CYL, and DHH carried out the measurements and data processing. CDC, CDM, and CYL analyzed data. CDC and CDM wrote the paper, with contributions from all coauthors.

Competing interests. The authors declare that they have no conflict of interest.TS9

Acknowledgements. This work was supported by the National Oceanic and Atmospheric Administration Atmospheric Chemistry, Carbon Cycle and Climate program, awards NA16OAR4310111 and NA16OAR4310112. CYL was additionally supported by the National Science Foundation Graduate Research Fellowship Program. The entire FIREX team, especially Bob Yokelson and Jim Roberts and the staff of the Missoula Fire Sciences Laboratory, is acknowledged for their assistance. Putting together the community inlet was a community effort – thank you to all who contributed. Shuka Schwarz and Gavin McMeeking are also thanked for their assistance with the SP2.

Financial support. This research has been supported by the National Oceanic and Atmospheric Administration’s Climate Program Office (grant nos. NA16OAR4310111 and NA16OAR4310112).TS10

Review statement. This paper was edited by Manabu Shiraiwa and reviewed by two anonymous referees.

References

- Adachi, K., Chung, S. H., and Buseck, P. R.: Shapes of soot aerosol particles and implications for their effects on climate, *J. Geophys. Res.*, 115, D15206, <https://doi.org/10.1029/2009jd012868>, 2010.
- 5 Aiken, A. C., Decarlo, P. F., Kroll, J. H., Worsnop, D. R., Huffman, J. A., Docherty, K. S., Ulbrich, I. M., Mohr, C., Kimmel, J. R., Sueper, D., Sun, Y., Zhang, Q., Trimborn, A., Northway, M., Ziemann, P. J., Canagaratna, M. R., Onasch, T. B., Alfarra, M. R., Prevot, A. S. H., Dommen, J., Duplissy, J., Metzger, A., Baltensperger, U., and Jimenez, J. L.: O/C and OM/OC ratios of primary, secondary, and ambient organic aerosols with high-resolution time-of-flight aerosol mass spectrometry, *Environ. Sci. Technol.*, 42, 4478–4485, <https://doi.org/10.1021/es703009q>, 2008.
- 15 Alfarra, M. R., Prevot, A. S. H., Szidat, S., Sandradewi, J., Weimer, S., Lanz, V. A., Schreiber, D., Mohr, M., and Baltensperger, U.: Identification of the Mass Spectral Signature of Organic Aerosols from Wood Burning Emissions, *Environ. Sci. Technol.*, 41, 5770–5777, <https://doi.org/10.1021/es062289b>, 2007.
- 20 Andreae, M. O. and Merlet, P.: Emission of trace gases and aerosols from biomass burning, *Global Biogeochem. Cy.*, 15, 955–966, <https://doi.org/10.1029/2000GB001382>, 2001.
- Bond, T. C. and Bergstrom, R. W.: Light absorption by carbonaceous particles: An investigative review, *Aerosol Sci. Tech.*, 40, 27–67, <https://doi.org/10.1080/02786820500421521>, 2006.
- 25 Bond, T. C., Habib, G., and Bergstrom, R. W.: Limitations in the enhancement of visible light absorption due to mixing state, *J. Geophys. Res.-Atmos.*, 111, <https://doi.org/10.1029/2006JD007315>, 2006.
- 30 Bond, T. C., Doherty, S. J., Fahey, D. W., Forster, P. M., Bernsten, T., DeAngelo, B. J., Flanner, M. G., Ghan, S., Kärcher, B., Koch, D., Kinne, S., Kondo, Y., Quinn, P. K., Sarofim, M. C., Schultz, M. G., Schulz, M., Venkataraman, C., Zhang, H., Zhang, S., Bellouin, N., Guttikunda, S. K., Hopke, P. K., Jacobson, M. Z., Kaiser, J. W., Klimont, Z., Lohmann, U., Schwarz, J. P., Shindell, D., Storelvmo, T., Warren, S. G., and Zender, C. S.: Bounding the role of black carbon in the climate system: A scientific assessment, *J. Geophys. Res.-Atmos.*, 118, 1–173, <https://doi.org/10.1002/jgrd.50171>, 2013.
- 40 Cappa, C. D., Onasch, T. B., Massoli, P., Worsnop, D., Bates, T. S., Cross, E., Davidovits, P., Hakala, J., Hayden, K., Jobson, B. T., Kolesar, K. R., Lack, D. A., Lerner, B., Li, S. M., Mellon, D., Nuanman, I., Olfert, J., Petaja, T., Quinn, P. K., Song, C., Subramanian, R., Williams, E. J., and Zaveri, R. A.: Radiative absorption enhancements due to the mixing state of atmospheric black carbon, *Science*, 337, 1078–1081, <https://doi.org/10.1126/science.1223447>, 2012.
- 45 Cappa, C. D., Lim, C. Y., Hagan, D. H., and Kroll, J. H.: Measurements from the Fire Influence on Regional and Global Environments Experiment (FIREX) Fire Lab Mini Chamber Experiment, UC Davis DASH, Dataset, Version 1, <https://doi.org/10.25338/B8CK5N>, 2019a.
- 50 Cappa, C. D., Zhang, X., Russell, L. M., Collier, S., Lee, A. K. Y., Chen, C.-L., Betha, R., Chen, S., Liu, J., Price, D. J., Sanchez, K. J., McMeeking, G., Williams, L. R., Onasch, T. B., Worsnop, D. R., Abbatt, J., and Zhang, Q.: Light absorption by ambient black and brown carbon and its dependence on black carbon coating state for two California, USA cities in winter and summer, *J. Geophys. Res.-Atmos.*, <https://doi.org/10.1029/2018JD029501>, 2019b. **TS11**
- Chakrabarty, R. K. and Heinson, W. R.: Scaling Laws for Light Absorption Enhancement Due to Nonrefractory Coating of Atmospheric Black Carbon Aerosol, *Phys. Rev. Lett.*, 121, 218701, <https://doi.org/10.1103/PhysRevLett.121.218701>, 2018.
- 60 Coggon, M. M., Lim, C. Y., Koss, A. R., Sekimoto, K., Yuan, B., Gilman, J. B., Hagan, D. H., Selimovic, V., Zarzana, K. J., Brown, S. S., Roberts, J. M., Müller, M., Yokelson, R., Wisthaler, A., Krechmer, J. E., Jimenez, J. L., Cappa, C., Kroll, J. H., de Gouw, J., and Warneke, C.: OH chemistry of non-methane organic gases (NMOGs) emitted from laboratory and ambient biomass burning smoke: evaluating the influence of furans and oxygenated aromatics on ozone and secondary NMOG formation, *Atmos. Chem. Phys.*, 19, 14875–14899, <https://doi.org/10.5194/acp-19-14875-2019>, 2019.
- 75 Cubison, M. J., Ortega, A. M., Hayes, P. L., Farmer, D. K., Day, D., Lechner, M. J., Brune, W. H., Apel, E., Diskin, G. S., Fisher, J. A., Fuelberg, H. E., Hecobian, A., Knapp, D. J., Mikoviny, T., Riemer, D., Sachse, G. W., Sessions, W., Weber, R. J., Weinheimer, A. J., Wisthaler, A., and Jimenez, J. L.: Effects of aging on organic aerosol from open biomass burning smoke in aircraft and laboratory studies, *Atmos. Chem. Phys.*, 11, 12049–12064, <https://doi.org/10.5194/acp-11-12049-2011>, 2011.
- 80 Fierce, L., Bond, T. C., Bauer, S. E., Mena, F., and Riemer, N.: Black carbon absorption at the global scale is affected by particle-scale diversity in composition, *Nat. Comm.*, 7, 12361, <https://doi.org/10.1038/ncomms12361>, 2016.
- 85 Forestieri, S. D., Helgestad, T. M., Lambe, A. T., Renbaum-Wolff, L., Lack, D. A., Massoli, P., Cross, E. S., Dubey, M. K., Mazoleni, C., Olfert, J. S., Sedlacek III, A. J., Freedman, A., Davidovits, P., Onasch, T. B., and Cappa, C. D.: Measurement and modeling of the multiwavelength optical properties of uncoated flame-generated soot, *Atmos. Chem. Phys.*, 18, 12141–12159, <https://doi.org/10.5194/acp-18-12141-2018>, 2018.
- 90 Fuller, K. A., Malm, W. C., and Kreidenweis, S. M.: Effects of mixing on extinction by carbonaceous particles, *J. Geophys. Res.-Atmos.*, 104, 15941–15954, <https://doi.org/10.1029/1998jd100069>, 1999.
- 95 Garofalo, L. A., Pothier, M. A., Levin, E. J. T., Campos, T., Kreidenweis, S. M., and Farmer, D. K.: Emission and Evolution of Submicron Organic Aerosol in Smoke from Wildfires in the Western United States, *ACS Earth Space Chem.*, 3, 1237–1247, <https://doi.org/10.1021/acsearthspacechem.9b00125>, 2019.
- 100 Healy, R., Wang, J., Jeong, C. H., Lee, A., Willis, M., Jaroudi, E., Zimmerman, N., Hilker, N., Murphy, M., and Eckhardt, S.: Light-absorbing properties of ambient black carbon and brown carbon from fossil fuel and biomass burning sources, *J. Geophys. Res.-Atmos.*, 120, 6619–6633, <https://doi.org/10.1002/2015JD023382>, 2015.
- 105 Hosseini, S., Li, Q., Cocker, D., Weise, D., Miller, A., Shrivastava, M., Miller, J. W., Mahalingam, S., Princevac, M., and Jung, H.: Particle size distributions from laboratory-scale biomass fires using fast response instruments, *Atmos. Chem. Phys.*, 10, 8065–8076, <https://doi.org/10.5194/acp-10-8065-2010>, 2010.
- 110 Jacobson, M. Z.: Strong radiative heating due to the mixing state of black carbon in atmospheric aerosols, *Nature*, 409, 695–697, <https://doi.org/10.1038/35055518>, 2001.
- 115

- Jen, C. N., Hatch, L. E., Selimovic, V., Yokelson, R. J., Weber, R., Fernandez, A. E., Kreisberg, N. M., Barsanti, K. C., and Goldstein, A. H.: Speciated and total emission factors of particulate organics from burning western US wildland fuels and their dependence on combustion efficiency, *Atmos. Chem. Phys.*, 19, 1013–1026, <https://doi.org/10.5194/acp-19-1013-2019>, 2019.
- Kiendler-Scharr, A., Mensah, A. A., Friese, E., Topping, D., Nemitz, E., Prevot, A. S. H., Äijälä, M., Allan, J., Canonaco, F., Canagaratna, M., Carbone, S., Crippa, M., Dall'Osto, M., Day, D. A., De Carlo, P., Di Marco, C. F., Elbern, H., Eriksson, A., Freney, E., Hao, L., Herrmann, H., Hildebrandt, L., Hillamo, R., Jimenez, J. L., Laaksonen, A., McFiggans, G., Mohr, C., O'Dowd, C., Otjes, R., Ovadnevaite, J., Pandis, S. N., Poulain, L., Schlag, P., Sellegri, K., Swietlicki, E., Tiitta, P., Vermeulen, A., Wahner, A., Worsnop, D., and Wu, H.-C.: Ubiquity of organic nitrates from nighttime chemistry in the European submicron aerosol, *Geophys. Res. Lett.*, 43, 7735–7744, <https://doi.org/10.1002/2016GL069239>, 2016.
- Kirchstetter, T. W., Novakov, T., and Hobbs, P. V.: Evidence that the spectral dependence of light absorption by aerosols is affected by organic carbon, *J. Geophys. Res.-Atmos.*, 109, D21208, <https://doi.org/10.1029/2004JD004999>, 2004.
- Kondo, Y., Matsui, H., Moteki, N., Sahu, L., Takegawa, N., Kajino, M., Zhao, Y., Cubison, M. J., Jimenez, J. L., Vay, S., Diskin, G. S., Anderson, B., Wisthaler, A., Mikoviny, T., Fuelberg, H. E., Blake, D. R., Huey, G., Weinheimer, A. J., Knapp, D. J., and Brune, W. H.: Emissions of black carbon, organic, and inorganic aerosols from biomass burning in North America and Asia in 2008, *J. Geophys. Res.*, 116, D08204, <https://doi.org/10.1029/2010jd015152>, 2011.
- Koss, A. R., Sekimoto, K., Gilman, J. B., Selimovic, V., Coggon, M. M., Zarzana, K. J., Yuan, B., Lerner, B. M., Brown, S. S., Jimenez, J. L., Krechmer, J., Roberts, J. M., Warneke, C., Yokelson, R. J., and de Gouw, J.: Non-methane organic gas emissions from biomass burning: identification, quantification, and emission factors from PTR-ToF during the FIREX 2016 laboratory experiment, *Atmos. Chem. Phys.*, 18, 3299–3319, <https://doi.org/10.5194/acp-18-3299-2018>, 2018.
- Lack, D. A., Cappa, C. D., Cross, E. S., Massoli, P., Ahern, A. T., Davidovits, P., and Onasch, T. B.: Absorption Enhancement of Coated Absorbing Aerosols: Validation of the Photo-Acoustic Technique for Measuring the Enhancement, *Aerosol Sci. Tech.*, 43, 1006–1012, <https://doi.org/10.1080/02786820903117932>, 2009.
- Lack, D. A., Bahreini, R., Langridge, J. M., Gilman, J. B., and Middlebrook, A. M.: Brown carbon absorption linked to organic mass tracers in biomass burning particles, *Atmos. Chem. Phys.*, 13, 2415–2422, <https://doi.org/10.5194/acp-13-2415-2013>, 2013.
- Laskin, A., Lin, P., Laskin, J., Fleming, L. T., and Nizkorodov, S.: Molecular Characterization of Atmospheric Brown Carbon, in: *Multiphase Environmental Chemistry in the Atmosphere*, ACS Symposium Series, 1299, American Chemical Society, 261–274, 2018.
- Levin, E. J. T., McMeeking, G. R., Carrico, C. M., Mack, L. E., Kreidenweis, S. M., Wold, C. E., Moosmüller, H., Arnott, W. P., Hao, W. M., Collett, J. L., and Malm, W. C.: Biomass burning smoke aerosol properties measured during Fire Laboratory at Missoula Experiments (FLAME), *J. Geophys. Res.-Atmos.*, 115, D18210, <https://doi.org/10.1029/2009JD013601>, 2010.
- Lim, C. Y., Hagan, D. H., Coggon, M. M., Koss, A. R., Sekimoto, K., de Gouw, J., Warneke, C., Cappa, C. D., and Kroll, J. H.: Secondary organic aerosol formation from the laboratory oxidation of biomass burning emissions, *Atmos. Chem. Phys.*, 19, 12797–12809, <https://doi.org/10.5194/acp-19-12797-2019>, 2019.
- Lin, P., Aiona, P. K., Li, Y., Shiraiwa, M., Laskin, J., Nizkorodov, S. A., and Laskin, A.: Molecular Characterization of Brown Carbon in Biomass Burning Aerosol Particles, *Environ. Sci. Technol.*, 50, 11815–11824, <https://doi.org/10.1021/acs.est.6b03024>, 2016.
- Liu, D. T., Whitehead, J., Alfarra, M. R., Reyes-Villegas, E., Spracklen, D. V., Reddington, C. L., Kong, S. F., Williams, P. I., Ting, Y. C., Haslett, S., Taylor, J. W., Flynn, M. J., Morgan, W. T., McFiggans, G., Coe, H., and Allan, J. D.: Black-carbon absorption enhancement in the atmosphere determined by particle mixing state, *Nat. Geosci.*, 10, 184–188, <https://doi.org/10.1038/ngeo2901>, 2017.
- Liu, S., Aiken, A. C., Arata, C., Dubey, M. K., Stockwell, C. E., Yokelson, R. J., Stone, E. A., Jayarathne, T., Robinson, A. L., DeMott, P. J., and Kreidenweis, S. M.: Aerosol single scattering albedo dependence on biomass combustion efficiency: Laboratory and field studies, *Geophys. Res. Lett.*, 41, 742–748, <https://doi.org/10.1002/2013GL058392>, 2013.
- Liu, S., Aiken, A. C., Gorkowski, K., Dubey, M. K., Cappa, C. D., Williams, L. R., Herndon, S. C., Massoli, P., Fortner, E. C., Chhabra, P. S., Brooks, W. A., Onasch, T. B., Worsnop, D. R., China, S., Sharma, N., Mazzoleni, C., Xu, L., L., N. N., Liu, D., Allan, J. D., Lee, J. D., Fleming, Z. L., Mohr, C., Zotter, P., Szidat, S., and Prevot, A. S. H.: Enhanced light absorption by mixed source black and brown carbon particles in UK winter, *Nat. Comm.*, 6, 8435, <https://doi.org/10.1038/ncomms9435>, 2015.
- Mann, G. W., Carslaw, K. S., Reddington, C. L., Pringle, K. J., Schulz, M., Asmi, A., Spracklen, D. V., Ridley, D. A., Woodhouse, M. T., Lee, L. A., Zhang, K., Ghan, S. J., Easter, R. C., Liu, X., Stier, P., Lee, Y. H., Adams, P. J., Tost, H., Lelieveld, J., Bauer, S. E., Tsigaridis, K., van Noije, T. P. C., Strunk, A., Vignati, E., Bellouin, N., Dalvi, M., Johnson, C. E., Bergman, T., Kokkola, H., von Salzen, K., Yu, F., Luo, G., Petzold, A., Heintzenberg, J., Clarke, A., Ogren, J. A., Gras, J., Baltensperger, U., Kaminski, U., Jennings, S. G., O'Dowd, C. D., Harrison, R. M., Beddows, D. C. S., Kulmala, M., Viisanen, Y., Ulevicius, V., Mihalopoulos, N., Zdimal, V., Fiebig, M., Hansson, H.-C., Swietlicki, E., and Henzing, J. S.: Intercomparison and evaluation of global aerosol microphysical properties among AeroCom models of a range of complexity, *Atmos. Chem. Phys.*, 14, 4679–4713, <https://doi.org/10.5194/acp-14-4679-2014>, 2014.
- May, A. A., McMeeking, G. R., Lee, T., Taylor, J. W., Craven, J. S., Burling, I., Sullivan, A. P., Akagi, S., Collett Jr., J. L., Flynn, M., Coe, H., Urbanski, S. P., Seinfeld, J. H., Yokelson, R. J., and Kreidenweis, S. M.: Aerosol emissions from prescribed fires in the United States: A synthesis of laboratory and aircraft measurements, *J. Geophys. Res.-Atmos.*, 119, 11826–11849, <https://doi.org/10.1002/2014JD021848>, 2014.
- McMeeking, G. R., Kreidenweis, S. M., Baker, S., Carrico, C. M., Chow, J. C., Collett, J. L., Hao, W. M., Holden, A. S., Kirchstetter, T. W., Malm, W. C., Moosmüller, H., Sullivan, A. P., and

- Wold, C. E.: Emissions of trace gases and aerosols during the open combustion of biomass in the laboratory, *J. Geophys. Res.-Atmos.*, 114, D19210, <https://doi.org/10.1029/2009JD011836>, 2009.
- 5 McMeeking, G. R., Fortner, E., Onasch, T. B., Taylor, J. W., Flynn, M., Coe, H., and Kreidenweis, S. M.: Impacts of non-refractory material on light absorption by aerosols emitted from biomass burning, *J. Geophys. Res.-Atmos.*, 119, 12272–12286, <https://doi.org/10.1002/2014JD021750>, 2014.
- 10 Mohr, C., Lopez-Hilfiker, F. D., Zotter, P., Prévôt, A. S. H., Xu, L., Ng, N. L., Herndon, S. C., Williams, L. R., Franklin, J. P., Zahniser, M. S., Worsnop, D. R., Knighton, W. B., Aiken, A. C., Gorkowski, K. J., Dubey, M. K., Allan, J. D., and Thornton, J. A.: Contribution of Nitrated Phenols to Wood Burning
- 15 Brown Carbon Light Absorption in Detling, United Kingdom during Winter Time, *Environ. Sci. Technol.*, 47, 6316–6324, <https://doi.org/10.1021/es400683v>, 2013.
- Peng, J., Hu, M., Guo, S., Du, Z., Zheng, J., Shang, D., Zamora, M. L., Zeng, L., Shao, M., Wu, Y.-S., Zheng, J., Wang, Y., Glen, C. R., Collins, D. R., Molina, M. J., and Zhang, R.: Markedly enhanced absorption and direct radiative forcing of black carbon under polluted urban environments, *P. Natl. Acad. Sci. USA*, 113, 4266–4271, <https://doi.org/10.1073/pnas.1602310113>, 2016.
- Pokhrel, R. P., Wagner, N. L., Langridge, J. M., Lack, D. A., Jayarathne, T., Stone, E. A., Stockwell, C. E., Yokelson, R. J., and Murphy, S. M.: Parameterization of single-scattering albedo (SSA) and absorption Ångström exponent (AAE) with EC/OC for aerosol emissions from biomass burning, *Atmos. Chem. Phys.*, 16, 9549–9561, <https://doi.org/10.5194/acp-16-9549-2016>, 2016.
- 30 Pokhrel, R. P., Beamesderfer, E. R., Wagner, N. L., Langridge, J. M., Lack, D. A., Jayarathne, T., Stone, E. A., Stockwell, C. E., Yokelson, R. J., and Murphy, S. M.: Relative importance of black carbon, brown carbon, and absorption enhancement from clear coatings in biomass burning emissions, *Atmos. Chem. Phys.*, 17, 5063–5078, <https://doi.org/10.5194/acp-17-5063-2017>, 2017.
- Reid, J. S., Koppmann, R., Eck, T. F., and Eleuterio, D. P.: A review of biomass burning emissions part II: intensive physical properties of biomass burning particles, *Atmos. Chem. Phys.*, 5, 799–825, <https://doi.org/10.5194/acp-5-799-2005>, 2005.
- 40 Sahu, L. K., Kondo, Y., Moteki, N., Takegawa, N., Zhao, Y., Cubison, M. J., Jimenez, J. L., Vay, S., Diskin, G. S., Wisthaler, A., Mikoviny, T., Huey, L. G., Weinheimer, A. J., and Knapp, D. J.: Emission characteristics of black carbon in anthropogenic and biomass burning plumes over California during ARCTAS-CARB 2008, *J. Geophys. Res.-Atmos.*, 117, D16302, <https://doi.org/10.1029/2011jd017401>, 2012.
- Saleh, R., Robinson, E. S., Tkacik, D. S., Ahern, A. T., Liu, S., Aiken, A. C., Sullivan, R. C., Presto, A. A., Dubey, M. K., Yokelson, R. J., Donahue, N. M., and Robinson, A. L.: Brownness of organics in aerosols from biomass burning linked to their black carbon content, *Nature Geosci.*, 7, 647–650, <https://doi.org/10.1038/ngeo2220>, 2014.
- 55 Saleh, R., Cheng, Z., and Atwi, K.: The Brown–Black Continuum of Light-Absorbing Combustion Aerosols, *Environ. Sci. Technol. Lett.*, 5, 508–513, <https://doi.org/10.1021/acs.estlett.8b00305>, 2018.
- Schneider, J., Weimer, S., Drewnick, F., Borrmann, S., Helas, G., Gwaze, P., Schmid, O., Andreae, M. O., and Kirchner, U.: Mass spectrometric analysis and aerodynamic properties of various types of combustion-related aerosol particles, *Int. J. Mass Spectrom.*, 258, 37–49, <https://doi.org/10.1016/j.ijms.2006.07.008>, 2006.
- Schwarz, J. P., Gao, R. S., Spackman, J. R., Watts, L. A., Thomson, D. S., Fahey, D. W., Ryerson, T. B., Peischl, J., Holloway, J. S., Trainer, M., Frost, G. J., Baynard, T., Lack, D. A., de Gouw, J. A., Warneke, C., and Del Negro, L. A.: Measurement of the mixing state, mass, and optical size of individual black carbon particles in urban and biomass burning emissions, *Geophys. Res. Lett.*, 35, L13810, <https://doi.org/10.1029/2008gl033968>, 2008.
- 70 Shiraiwa, M., Kondo, Y., Iwamoto, T., and Kita, K.: Amplification of Light Absorption of Black Carbon by Organic Coating, *Aerosol Sci. Tech.*, 44, 46–54, <https://doi.org/10.1080/02786820903357686>, 2010.
- Zhang, X., Kim, H., Parworth, C., Young, D. E., Zhang, Q., Metcalf, A. R., and Cappa, C. D.: Optical Properties of Wintertime Aerosols from Residential Wood Burning in Fresno, CA: Results from DISCOVER-AQ 2013, *Environ. Sci. Technol.*, 50, 1681–1690, <https://doi.org/10.1021/acs.est.5b04134>, 2016.

Remarks from the language copy-editor

- CE1** **INTERNAL. Please note title change.**
- CE2** Please verify that this is correct. Should "sizer" be "spectrometer"?
- CE3** Should this be ceanothus?
- CE4** Please define.

Remarks from the typesetter

- TS1** Please provide additional information for all affiliations where applicable; e.g. department.
- TS2** Please check, I noticed that your paper is not registered as a companion paper in our system, so please let me know if we can delete "Part 1" in the title.
- TS3** The composition of all Figures and the key figure has been adjusted to our standards. This also includes language adjustments to all Figures.
- TS4** Please add last access date.
- TS5** Please note that units have been changed to exponential format. Please check all instances.
- TS6** Please confirm.
- TS7** Please confirm.
- TS8** Please provide a reference list entry including creators, title, and date of last access.
- TS9** Declaration of all potential conflicts of interest is required by us as this is an integral aspect of a transparent record of scientific work. If there are possible conflicts of interest, please state what competing interests are relevant to your work.
- TS10** Please note that the funding information has been added to this paper. Please check if it is correct. Please also double-check your acknowledgements to see whether repeated information can be removed or changed accordingly. Thanks.
- TS11** Please add page range or article number.